Eur. Phys. J. A (2011) **47**: 63
DOI 10.1140/epja/i2011-11063-x

**THE EUROPEAN PHYSICAL JOURNAL A**

Regular Article – Experimental Physics

# pp and $\pi\pi$ intensity interferometry in collisions of Ar+KCl at 1.76A GeV

The HADES Collaboration

G. Agakishiev[8], A. Balanda[3†], B. Bannier[5], R. Bassini[9], D. Belver[15], A.V. Belyaev[6], A. Blanco[2], M. Böhmer[11], J.L. Boyard[13], P. Cabanelas[15], E. Castro[15], S. Chernenko[6], T. Christ[11], M. Destefanis[8], J. Díaz[16], F. Dohrmann[5], A. Dybczak[3], T. Eberl[11], E. Epple[11], L. Fabbietti[11,17], O.V. Fateev[6], P. Finocchiaro[1], P. Fonte[2,18], J. Friese[11], I. Fröhlich[7], T. Galatyuk[7], J.A. Garzón[15], R. Gernhäuser[11], A. Gil[16], C. Gilardi[8], M. Golubeva[10], D. González-Díaz[4], F. Guber[10], M. Gumberidze[13], M. Heilmann[7], T. Heinz[4], T. Hennino[13], R. Holzmann[4], P. Huck[11], I. Iori[9,19†], A. Ivashkin[10], M. Jurkovic[11], B. Kämpfer[5,20], K. Kanaki[5], T. Karavicheva[10], D. Kirschner[8], I. Koenig[4], W. Koenig[4], B.W. Kolb[4], R. Kotte[5,a], F. Krizek[14], R. Krücken[11], W. Kühn[8], A. Kugler[14], A. Kurepin[10], S. Lang[4], J.S. Lange[8], K. Lapidus[10,17], T. Liu[13], L. Lopes[2], M. Lorenz[7], L. Maier[11], A. Mangiarotti[2], J. Markert[7], V. Metag[8], B. Michalska[3], J. Michel[7], D. Mishra[8], E. Morinière[13], J. Mousa[12], C. Müntz[7], L. Naumann[5], J. Otwinowski[3], Y.C. Pachmayer[7], M. Palka[4], Y. Parpottas[12], V. Pechenov[4], O. Pechenova[8], T. Pérez Cavalcanti[8], J. Pietraszko[4], W. Przygoda[3], B. Ramstein[13], A. Reshetin[10], M. Roy-Stephan[13], A. Rustamov[4], A. Sadovsky[10], B. Sailer[11], P. Salabura[3], A. Schmah[11,21], E. Schwab[4], J. Siebenson[11], Yu.G. Sobolev[14], S. Spataro[8,22], B. Spruck[8], H. Ströbele[7], J. Stroth[7,4], C. Sturm[4], A. Tarantola[7], K. Teilab[7], P. Tlusty[14], M. Traxler[4], R. Trebacz[3], H. Tsertos[12], V. Wagner[14], M. Weber[11], C. Wendisch[5], M. Wisniowski[3], T. Wojcik[3], J. Wüstenfeld[5], S. Yurevich[4], Y.V. Zanevsky[6], P. Zhou[5], and P. Zumbruch[4]

[1] Istituto Nazionale di Fisica Nucleare - Laboratori Nazionali del Sud, 95125 Catania, Italy
[2] LIP-Laboratório de Instrumentação e Física Experimental de Partículas, 3004-516 Coimbra, Portugal
[3] Smoluchowski Institute of Physics, Jagiellonian University of Cracow, 30-059 Kraków, Poland
[4] GSI Helmholtzzentrum für Schwerionenforschung GmbH, 64291 Darmstadt, Germany
[5] Institut für Strahlenphysik, Helmholtz-Zentrum Dresden-Rossendorf, 01314 Dresden, Germany
[6] Joint Institute of Nuclear Research, 141980 Dubna, Russia
[7] Institut für Kernphysik, Johann Wolfgang Goethe-Universität, 60438 Frankfurt, Germany
[8] II.Physikalisches Institut, Justus Liebig Universität Giessen, 35392 Giessen, Germany
[9] Istituto Nazionale di Fisica Nucleare, Sezione di Milano, 20133 Milano, Italy
[10] Institute for Nuclear Research, Russian Academy of Science, 117312 Moscow, Russia
[11] Physik Department E12, Technische Universität München, 85748 München, Germany
[12] Department of Physics, University of Cyprus, 1678 Nicosia, Cyprus
[13] Institut de Physique Nucléaire (UMR 8608), CNRS/IN2P3 - Université Paris Sud, F-91406 Orsay Cedex, France
[14] Nuclear Physics Institute, Academy of Sciences of Czech Republic, 25068 Rez, Czech Republic
[15] Departamento de Física de Partículas, Universidad de Santiago de Compostela, 15706 Santiago de Compostela, Spain
[16] Instituto de Física Corpuscular, Universidad de Valencia-CSIC, 46971 Valencia, Spain
[17] Excellence Cluster Universe, Technische Universität München, 85748 Garching, Germany
[18] ISEC Coimbra, Coimbra, Portugal
[19] Dipartimento di Fisica, Università di Milano, 20133 Milano, Italy
[20] Technische Universität Dresden, 01062 Dresden, Germany
[21] Lawrence Berkeley National Laboratory, Berkeley CA 94720, USA
[22] Dipartimento di Fisica Generale, Università di Torino, 10125 Torino, Italy

Received: 28 October 2010 / Revised: 1 February 2011
Published online: 20 May 2011

Communicated by C. Signorini

**Abstract.** Results on pp, $\pi^+\pi^+$, and $\pi^-\pi^-$ intensity interferometry are reported for collisions of Ar+KCl at 1.76$A$ GeV beam energy, studied with the High Acceptance Di-Electron Spectrometer (HADES) at SIS18/GSI. The experimental correlation functions as a function of the relative momentum are compared to model calculations allowing the determination of the space-time extent of the corresponding emission sources. The $\pi\pi$ source radii are found significantly larger than the pp emission radius. The present radii do well complement the beam-energy dependences of Gaussian source radii of the collision system of size $A + A \simeq 40 + 40$. The pp source radius at fixed beam energy is found to increase linearly with the cube root of the number of participants. From this trend, a lower limit of the pp correlation radius is deduced.

## 1 Introduction

Two-particle intensity interferometry of hadrons is widely used to study the spatio-temporal size, shape and evolution of their source created in heavy-ion collisions or other reactions involving hadrons (for a review see ref. [1]). The technique, pioneered by Hanbury Brown and Twiss [2] to measure angular radii of stars, later on named HBT interferometry, is based on the quantum-statistical interference of identical particles. Goldhaber *et al.* [3] first applied intensity interferometry to hadrons. In heavy-ion collisions, the intensity interferometry does not allow to measure directly the reaction volume, as the emission sources, changing in shape and size in the course of the collision, may be affected by density and temperature gradients and dynamically generated space-momentum correlations (*e.g.*, radial expansion after the compression phase). Thus, intensity interferometry generally does not yield the proper source size, but rather an effective "length of homogeneity" [1]. It describes source volumes in which particle pairs are close in momentum, so that they are correlated as a consequence of their quantum statistics or due to their two-body interaction. At intermediate energies, various emission processes cause a broad band of origins of the measured particles. Therefore, the intensity interferometry may provide additional information to the understanding of reaction mechanisms which finally determine the particle emission sources. To obtain a reasonable picture of the complex heavy-ion collision the usage of different particle probes is mandatory. In general, the sign and strength of the correlation is affected by i) the strong interaction, ii) the Coulomb interaction if charged particles are involved, and iii) the quantum statistics in the case of identical particles (Pauli suppression for fermions, Bose-Einstein enhancement for bosons). Their interplay leads, for example, to rather complex pp correlation functions, with a characteristic dip + peak shape [4], showing a suppression at very low relative momenta (owing to items ii) and iii)) followed by a maximum that results from the short-range attractive strong interaction. In the case of $\pi\pi$ correlations, the mutual strong interaction appears to be minor [5] compared to the effects ii) and iii).

In this article we report on the investigation of pp, $\pi^+\pi^+$ and $\pi^-\pi^-$ correlations at low relative momenta in collisions of Ar+KCl at a beam kinetic energy of 1.76$A$ GeV. (A corresponding $\Lambda$p-correlation analysis for the same experiment has already been presented in ref. [6].) In sect. 2 we shortly describe the experiment. In sect. 3 we define the correlation function and discuss possible distortions to it. In sect. 4 we present the emission source radii resulting from the correlation analysis and compare them to the findings of other experiments. Finally, we summarize our results in sect. 5.

## 2 The experiment

The experiment was performed with the High Acceptance Di-Electron Spectrometer (HADES) at the Schwerionen-synchrotron SIS18 at GSI, Darmstadt. HADES, although primarily designed to measure di-electrons [7], offers excellent hadron identification capabilities [8–12] allowing for a profound proton and pion intensity interferometry. A detailed description of the spectrometer is presented in ref. [13]. In the following we summarize the main features of the apparatus.

HADES consists of a 6-coil toroidal magnet centered on the beam axis and six identical detection sections located between the coils and covering polar angles from 18° to 85°. The six sectors consisted of hadron blind Ring-Imaging Cherenkov (RICH) detectors (not used for the present investigation), four planes of Multi-wire Drift Chambers (MDCs) for track reconstruction (with two opposite MDCs in the outermost plane not installed during the present experiment), and two time-of-flight walls (TOF and TOFino), supplemented at forward polar angles with Pre-Shower chambers. The TOF and TOFino+Pre-Shower detectors were combined into a Multiplicity and Electron Trigger Array (META). A reconstructed track in the spectrometer is composed of straight inner and outer track segments in the MDCs. The pointing vector of the outer track segment is used for matching with a META hit. Possible trajectories through two track segments are combined to track candidates. A Runge-Kutta algorithm allows to calculate the momentum of each track candidate making use of the track deflection in the magnetic field. The quality of the META-hit matching and the Runge-Kutta fitting (characterized by $\chi^2$ values) is used to create a list of ordered track candidates. The track candidate with the lowest product of both $\chi^2$ values is selected as the true track. Its components and associated track candidates are then deleted from the candidate list. This procedure is repeated until no track candidates are left in the list. Particle identification of $\pi^\pm$ and protons is based on the correlation of their momenta and velocities. The particle velocity is determined by the time of flight between a diamond start detector and the hit on the META detectors and by the reconstructed flight path. At forward polar angles, where the particle identification suffers from multiple detector hits and poorer TOF resolution, in addition the correlation of momentum and energy loss of the particle in the MDCs is taken into account. Graphical cuts in the corresponding correlation plots are used to select the different particle species [8,12].

A $^{40}$Ar beam of about $10^6$ particles per second with kinetic energy of 1.76$A$ GeV was incident on a four-fold segmented target of natural KCl with a segment interval of 8 mm and a total thickness of 5 mm corresponding to 3.3% interaction length. The position resolution (sigma) of the reaction vertex amounts to 0.3 mm in both transverse directions while in beam direction it amounts to 1.5 mm. The data readout was started by a first-level trigger (LVL1) decision, requiring a charged-particle multiplicity $\geq$ 16 in the TOF/TOFino detectors. The integrated cross-section selected by this trigger comprises approximately the most central 35% of the total reaction cross-section. About 700 million LVL1 events were processed for the present investigation.

[a] e-mail: kotte@fzd.de
[†] Deceased.

In previous proton-proton correlation analyses of experiments conducted by the FOPI collaboration [14–17] an enhanced coincidence yield at very low relative angles was observed. It was traced back to coincident signals from neighbouring plastic scintillation strips of the time-of-flight wall which were generated by the same charged particle. A similar double-counting effect, either caused by a slight geometrical overlap of the scintillators w.r.t. the inclined track direction or by scattering of particles from one to another strip, might be expected for HADES, too. However, this disturbing yield is reduced strongly by the requirement to match the particle hits on the META detectors with the corresponding tracks derived from the position information of the drift chambers. Remainders of doubly counted scattered particles, possibly matched with fake tracks, are eliminated by excluding close track pairs appearing within an opening angle of less than 3° (5°) for proton (pion) pairs. This procedure takes also care of the opposite effect of a possible deficit at low relative momenta due to the finite capability of the detector and the corresponding tracking software to resolve close tracks. The same selection is applied to the uncorrelated background, hence keeping the influence onto the correlation function negligible (see sect. 3). The lower limits for the opening angle have been chosen by compromising on the elimination of the detector bias at very low relative momenta and on event statistics for the analysis of the correlation function. The cut was optimized by increasing the minimum opening angle until the interesting region of the correlation function, that is, the peak in the two-proton case, showed no further distortion.

## 3 Correlation function

Generally, the two-particle correlation function is defined [1] as the ratio of the probability to measure simultaneously two particles with momenta $\mathbf{p}_1$ and $\mathbf{p}_2$ and the product of the corresponding single-particle probabilities,

$$\mathrm{C}(\mathbf{p}_1, \mathbf{p}_2) = \frac{P_2(\mathbf{p}_1, \mathbf{p}_2)}{P_1(\mathbf{p}_1) P_1(\mathbf{p}_2)} \,. \tag{1}$$

Experimentally, this correlation function is calculated from the ratio of true and background yields, $Y_{true}(\mathbf{p}_1, \mathbf{p}_2)$ and $Y_{mix}(\mathbf{p}_1, \mathbf{p}_2)$, respectively, representing the sums over all events and over all pairs satisfying certain conditions. The uncorrelated background, denoted by the subscript "mix", is generated by event mixing, where particle 1 and particle 2 were taken from different events with reaction vertices corresponding to the same target segment (determined by the minimum distance to the next segment center) and of the same multiplicity class. For a reasonable classification, the multiplicity distribution of charged particles (combining the information from the META detectors and the inner two planes of drift chambers) is divided into six intervals of 8 units each, and one almost empty interval for multiplicities above 48 [8]. This choice guarantees that only events with comparable impact parameters are mixed. The six-dimensional correlation function is projected onto one half of the Lorentz-invariant relative momentum,

$$q = \tfrac{1}{2}\sqrt{(\mathbf{p}_1 - \mathbf{p}_2)^2 - (E_1 - E_2)^2}, \tag{2}$$

where $E_i = \sqrt{p_i^2 + m_i^2}$ and $m_i$ ($i = 1, 2$) are the total energies and the rest masses of the particles composing the pair, respectively. (We use units with $\hbar = c = 1$.) Note that for two particles of equal mass, $q$ is identical to the magnitude of the single momenta in the rest frame of the pair. Hence, the experimental correlation function is given by

$$\mathrm{C}_{exp}(q) = \mathcal{N}\,\frac{Y_{true}(q)}{Y_{mix}(q)}\,, \tag{3}$$

where $\mathcal{N}$ is a normalization factor (see below).

In previous investigations [18,19] of central Au + Au collisions between $100A$ and $400A$ MeV beam energy it was found that the correlation function of pairs of intermediate mass fragments is affected by the collective directed sideward flow of nuclear matter. This preferential emission of particles around the reaction plane may cause an enhancement of correlations at low relative momenta. The enhancement results from the creation of the reference distribution if differently azimuthally oriented events are mixed; it vanishes if the events are rotated into a unique reaction plane, which usually is determined by the transverse momentum analysis [20]. However, the technique of event rotation could not be applied to the present data due to the poor reaction-plane resolution limited by both, the small number of charged particles produced in the Ar+KCl collision and the limited fraction of observed particles (see sect. 4.1). On the other hand, the directed flow is known to be small for small systems [21]. Therefore, such an azimuthal anisotropy is expected to be reflected in the mixed $q$ distribution only as slightly larger width w.r.t. that of the true yield. Thus, instead of taking the ratio of total true and mixed yields, the normalization factor $\mathcal{N}$ in eq. (3) is fixed by the requirement $\mathrm{C}(q) \to 1$ at relative momenta of $q \sim (80 - 100)\,\mathrm{MeV}/c$, where the correlation function is expected to flatten out at unity. The statistical errors of $\mathrm{C}(q)$ are dominated by those of the true yield, since the mixed yield is generated with much higher statistics.

In case of pp correlations, where the source size is inversely correlated with the height of the correlation peak, the purity of the proton sample of $\epsilon_p = 0.95 \pm 0.02$ is taken into account [6,8]. The feeding from weak decays is neglected, considering that the mid-rapidity yield fraction of protons from $\Lambda$ decays amounts to 0.002 only [8, 22]. Hence, we correct the two-proton correlation function according to $\mathrm{C}(q) = (\mathrm{C}_{exp}(q) - 1)/\epsilon_p^2 + 1$, where $\epsilon_p^2$ is the pair purity. The result of the correction is a decrease of the pp source radius by about 0.1 fm. For $\pi^+\pi^+$ and $\pi^-\pi^-$ correlations, the pair impurity is covered by one of the fit parameters of the model correlation function (cf. sect. 4).

The influence of the finite momentum and position resolutions on the pp correlation function was determined with GEANT [23] simulations using PLUTO [24] as event generator. For a di-proton, decaying into two protons with

relative momenta of $q = 20\,\mathrm{MeV}/c$ (corresponding to the maximum of the pp correlation function), we found a relative-momentum resolution of $\delta q = (4\pm1)\,\mathrm{MeV}/c$. This resolution is taken into account by convoluting a Gaussian probability function of dispersion $\delta q$ with the theoretical pp correlation function calculated with the Koonin model [4]. The latter we will use to interpret the experimental two-proton correlations. Considering the momentum resolution leads to a decrease of the pp source radius by about 0.2 fm (see sect. 4). A similar correction to the two-pion correlation functions results in a slight increase of the source radii by less than 0.1 fm.

## 4 Results

### 4.1 Inclusive phase-space distributions

Figure 1 shows the experimental phase-space distributions of protons (top), $\pi^+$ (center), and $\pi^-$ (bottom) mesons in the plane of transverse momentum ($p_t$) *vs.* rapidity ($y = \tanh^{-1}(p_\parallel/E)$, where $p_\parallel$ is the longitudinal momentum along the beam direction). The missing acceptances in the upper right corners of the figure panels result from the upper momentum limits of the primary particle identification windows, *i.e.* 2.5, 1.95, and 2.2 GeV/$c$ for p, $\pi^+$, and $\pi^-$, respectively [8]. Note that for negative particles (the $\pi^-$) a narrow band of reduced acceptance appears, corresponding to those particles which are deflected by the toroidal magnetic field outwards into the gap between the two different systems of time-of-flight detectors (where the inner one, TOFino, is arranged behind the outer one, TOF). Here we emphasize the large acceptance of the HADES spectrometer which covers large parts of the phase space populated by the pions. On average, HADES detects about 12 protons, 1.7 $\pi^+$, and 2.1 $\pi^-$ mesons per LVL1 event, representing about 54%, 56%, and 54% of the corresponding total yields, respectively [8, 25]. While pions show broad distributions centered around mid-rapidity, $y_{cm} = 0.858$, the protons entering the correlation analysis, as a result of the detector acceptance and reconstruction efficiency, mostly originate from the region between target rapidity and mid-rapidity.

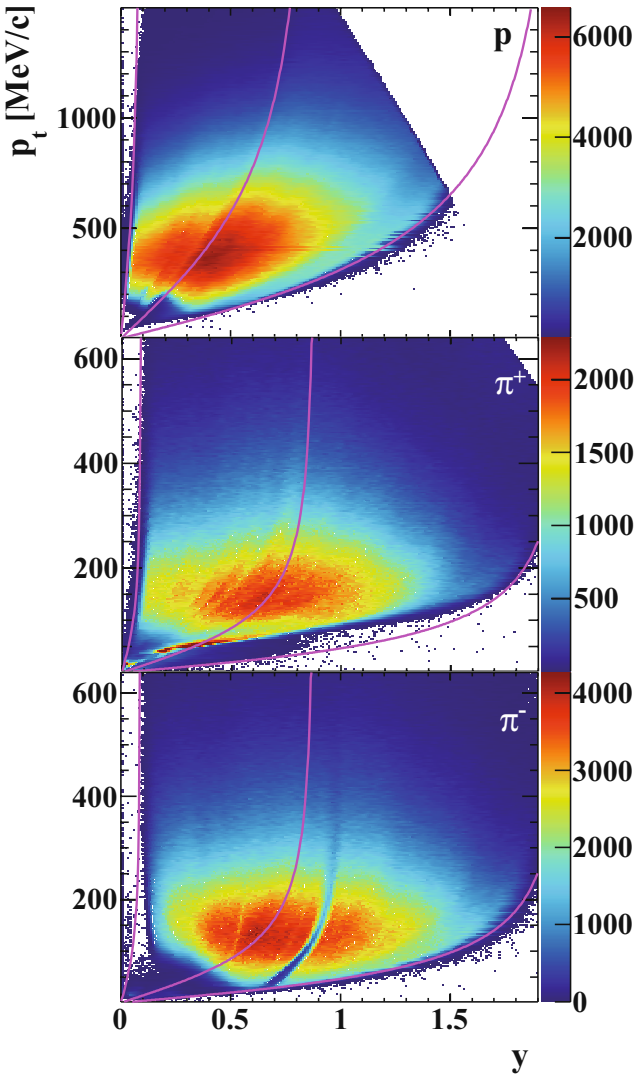


**Fig. 1.** Top: The distribution of single protons in the plane of transverse momentum *vs.* rapidity. The curves represent constant polar angles in the laboratory system of 15°, 45°, and 85° (from right to left). Center (bottom): The same, but for $\pi^+$ ($\pi^-$) mesons.

### 4.2 Source radii for LVL1 events

The overall correlation functions are displayed in fig. 2 together with the best fits of the model correlation functions (solid curves), using Koonin model [4] curves for pp correlations and Gaussian functions for the quantum-statistical part of the $\pi^+\pi^+$ and $\pi^-\pi^-$ correlations,

$$\mathrm{C}_{qs}(q) = 1 + e^{-R^2(2q)^2}. \quad (4)$$

The influence of the mutual Coulomb interaction is separated from the two-pion correlation functions by including in the fits the state-of-the-art Coulomb correction by Sinyukov *et al.* [26],

$$\mathrm{C}(q) = N\left[(1-\lambda) + \lambda\tilde{A}_c(q)\mathrm{C}_{qs}(q)\right]. \quad (5)$$

Here, the finite-size Coulomb factor $\tilde{A}_c$ results from the integration of the two-pion Coulomb wave function squared over a spherical Gaussian source of fixed radius. The latter is iteratively approximated by the result of the corresponding fit to the correlation function. The parameters $N$ and $\lambda$ in (5) represent a normalization constant and the fraction of femtoscopic pairs, respectively. Non-femtoscopic pairs consist of misidentified particles (about 5% [8]) and particles emitted too far from the source for the correlation to be resolved experimentally, *e.g.* due to feeding from $\eta$ and weak decays (about 2% [22,27]). The fit results in $\lambda = 0.45\pm0.01$ ($0.46\pm0.01$) for $\pi^+\pi^+$ ($\pi^-\pi^-$) correlations. Since, in the present paper, we concentrate on source sizes, $\lambda$ is not further discussed.

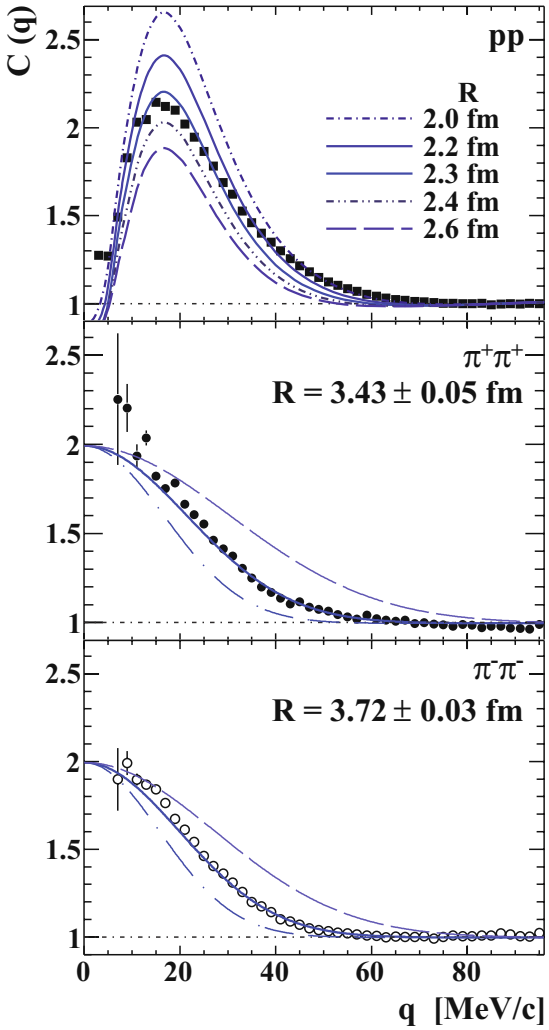


**Fig. 2.** Top: The overall pp correlation function as function of the invariant relative momentum. Error bars are statistical only. The solid curve indicates a fit with the Koonin model [4], while the other curves are calculations involving Gaussian source radii deviating from the best-fit value by $\pm 0.1$ and $\pm 0.3$ fm. Center (bottom): The quantum-statistical part of the overall $\pi^+\pi^+$ ($\pi^-\pi^-$) correlations. The solid curves display model correlation functions (eq. (4)) with the given Gaussian radii. The dashed and dash-dotted curves represent radii deviating from the best-fit value by $-1$ and $+1$ fm, respectively.

**Table 1.** The overall Gaussian source radius $R$ (in fm) and its uncertainties, derived from fitting the two-pion correlation functions with function (5) and the two-proton correlation function with the output of the Koonin model [4]. For completeness, also the p$\Lambda$ radius reported in [6] is given.

| Particle pair | p$\Lambda$ | pp | $\pi^+\pi^+$ | $\pi^-\pi^-$ |
|---|---|---|---|---|
| fit value | 2.09 | 2.29 | 3.43 | 3.72 |
| stat. error | $\pm 0.16$ | $\pm 0.02$ | $\pm 0.05$ | $\pm 0.03$ |
| syst. error | $^{+0.17}_{-0.22}$ | $^{+0.24}_{-0.16}$ | $^{+0.20}_{-0.18}$ | $^{+0.17}_{-0.18}$ |

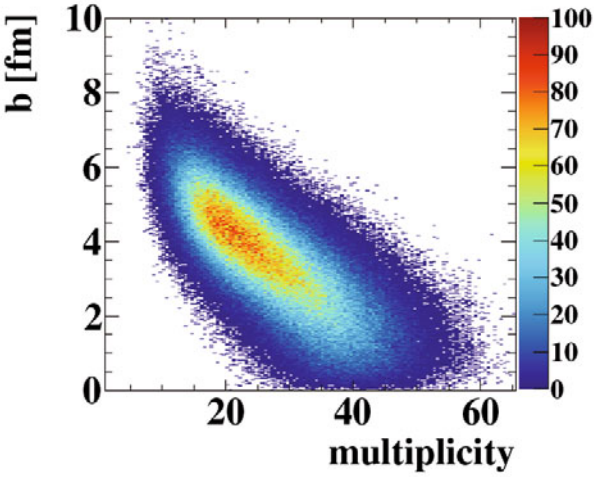


**Fig. 3.** The impact parameter $b$ *vs.* multiplicity of charged particles in the HADES acceptance as derived from GEANT [23] simulations using as event generator the UrQMD transport approach [28,29].

The best-fit values of the Gaussian source radii and the corresponding statistical and systematic errors are summarized in table 1. The quadratically added systematic errors mainly arise from the uncertainty of the close-track correction by demanding a minimum opening angle, from the uncertainty in the estimate of the relative-momentum resolution, from the choice of the fit range, and, for pp correlations, from the uncertainty of the purity correction.

The pp source radius is found slightly larger than the $\Lambda$p correlation radius recently derived [6] from the same data sample of Ar+KCl collisions and given in table 1, too. Also, for pp correlations we find some deficit of the model curves to describe the shape of the correlation function slightly beyond the maximum. This finding lets us argue that the proton source density distribution is not really spherical and of Gaussian shape as assumed in the model. Obviously, the dynamics of heavy-ion collisions at finite impact parameters leads to a temporal superposition of quite complex spatial shapes [17].

The Gaussian source radii derived from two-pion correlations are significantly larger than the radius obtained from pp correlations, potentially due to different emission durations. As these radii represent effective source extensions they comprise the temporal duration besides the spatial dimension (see sect. 4.4).

### 4.3 Centrality dependence

In a next step we studied the centrality dependence of pp and $\pi\pi$ correlation radii. For that purpose, five consecutive intervals of charged-particle multiplicity ($\leq 16$, 17–25, 26–34, 35–43, $\geq 44$) carrying sufficient statistics are selected and translated into impact parameter regions using GEANT simulations with the UrQMD [28,29] transport approach as event generator (see fig. 3). The average value and the width of the corresponding impact parameter distribution amount to 3.5 and 1.5 fm, respectively.

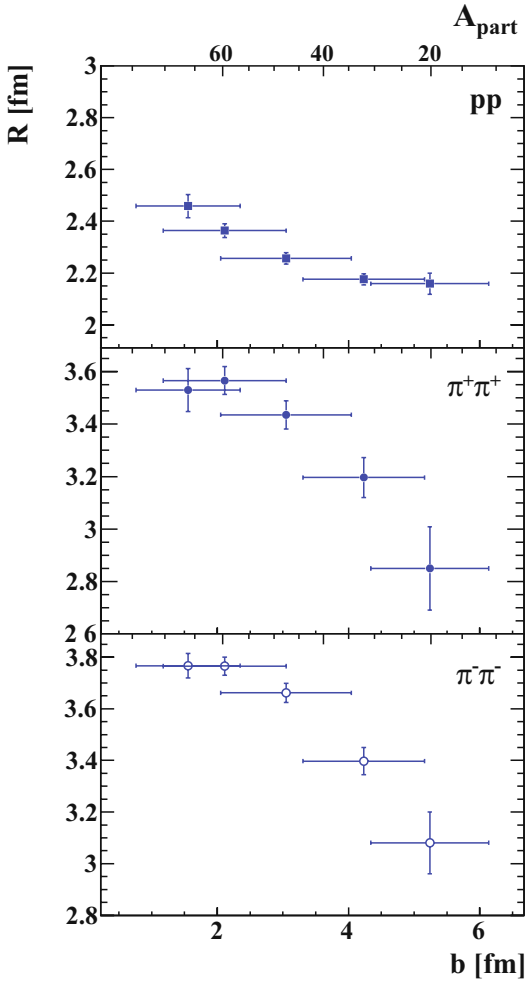


**Fig. 4.** The centrality dependence of the Gaussian source radius from pp (top), $\pi^+\pi^+$ (center), and $\pi^-\pi^-$ (bottom) correlations. The impact parameter range is calculated from consecutive multiplicity intervals, mapped on the impact parameter by the UrQMD transport approach (cf. fig. 3). The vertical error bars are statistical, while the horizontal ones represent the $1\sigma$ spread of the impact parameter distribution for the corresponding multiplicity windows. The upper abscissa shows the corresponding number of participants, calculated with a geometrical model of penetrating sharp spheres.

The corresponding mean number of participants resulting from calculations with a geometrical model of penetrating sharp spheres [30] amounts to $A_{part} = 38.5 \pm 2.5$ [25].

The result is displayed in fig. 4. For all three correlations an explicit trend of decreasing source radii with increasing impact parameter is evident, indicating the positive correlation of the source size with the overlap volume of the colliding nuclei. Note, however, that the magnitude of this variation is small. It amounts only to a few tenths of a femtometer. For small impact parameters a saturation of the emission source radii is observed. One may argue in fact that, by selecting very large multiplicities of charged particles, no further increase of the centrality can be achieved for small collision systems such as Ar+KCl due to the poor correlation of the impact parameter and multiplicity (cf. fig. 3).

### 4.4 Comparison to other experiments

The present emission source sizes may be compared to the data obtained by other experiments. In fig. 5 we show an excitation function of pp and $\pi^-\pi^-$ (Gaussian) source radii from central heavy-ion collisions of various systems. Typically, the event selection comprises the most central 10 to 20% of the total cross-section for large and small system sizes, respectively. To allow for a reliable comparison with our data, we choose (by interpolation) the correlation radii corresponding to a mean impact parameter of about 2.5 fm, that is, for a centrality of about 20%. To guide the eye and for the purpose of interpolation (see below), the source radii for symmetric systems of masses of $A + A \simeq 40 + 40$, $100 + 100$, and $200 + 200$, respectively, are connected by dashed curves, which are derived from linear regressions to the corresponding data. The present HADES data (full red circles) do indeed well complement the beam energy dependences of source radii for mass $40 + 40$ collision systems. For all system sizes and both types of particle pairs the source radius decreases with increasing beam energy. This shrinking of the apparent source may be traced back to the following effects. At higher beam energies, when the heavy-ion collisions is progressing faster, the contribution of the emission duration $\tau$ to the source extent is smaller. For finite values of $\tau$, the phase-space distribution of the emitted particles is elongated in the direction of the pair velocity $\mathbf{V}$, resulting in an effective source radius $R = \sqrt{R_0^2 + (V\tau)^2}$, where $R_0$ and $V\tau$ represent its spatial and temporal components, respectively. For the reaction energies in the present investigation, these emission durations (sometimes called "lifetimes") are in the order of few fm/$c$ [28,29]. Secondly, also the collective (radial) expansion found in central heavy-ion collisions becomes more pronounced with increasing projectile energies. It is well known [1,31] that strong correlations of coordinate and momentum space lead to a reduction of the apparent source radius. However, small collision systems like Ar+KCl exhibit only very small radial flow [32]. Hence, we neglect its influence onto the correlation function.

Taking interpolated values at $1.93A$ GeV following from the three regression lines in the upper panel of fig. 5 and the single data point of the pp source radius for Ni+Ni taken at this beam energy, we investigated the system size dependence of the pp source radius for a fixed beam energy. Figure 6 shows radii as a function of the cube root of the number of participants $A_{part}^{1/3}$. Also here, $A_{part}$ follows from the geometrical model using the corresponding collision centralities and system sizes. Obviously, the pp radii exhibit a common trend. Following the almost linear dependence down to $A_{part} = 1$, we deduce a lower limit of the Gaussian pp correlation radius of about $(0.36 \pm 0.45)$ fm (statistical error given). A very similar, almost linear, dependence on $A_{part}^{1/3}$ was found

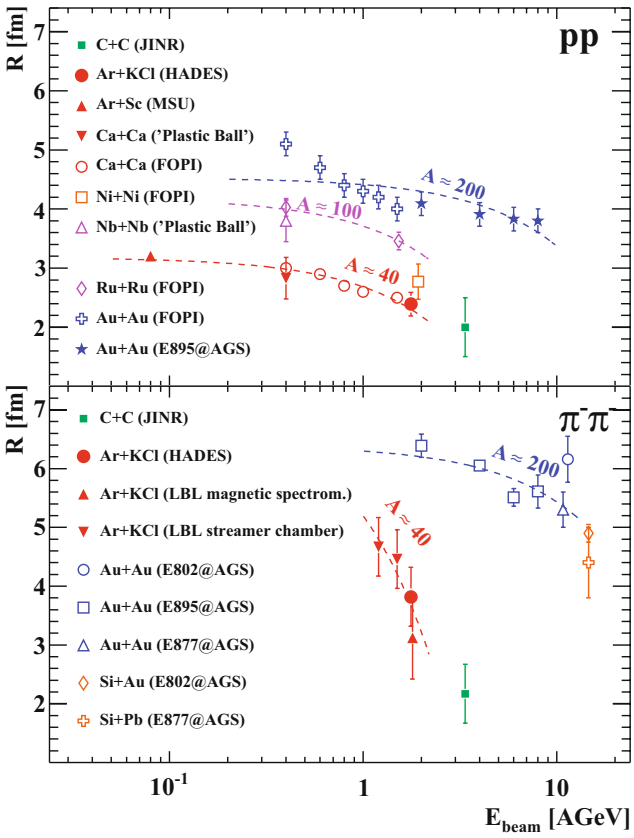


**Fig. 5.** (Color online) Top: The Gaussian source radius as derived from pp correlation functions in symmetric central heavy-ion collisions as a function of beam energy. The full red circle represent the HADES data. The other symbols given in the legend correspond to data of JINR [35], MSU [36], Plastic Ball [37], FOPI [14–17], E895 [38,39]. The various dashed curves are linear regressions to the data of the collision systems with sizes of $A + A \simeq 40 + 40$, $100 + 100$, and $200 + 200$. Bottom: The same, but for $\pi^-\pi^-$ correlation radii and for collision systems of size $A + A \simeq 40 + 40$ and $200 + 200$ (also including a few asymmetric systems). Further references: JINR [35], LBL magnetic spectrometer [40], LBL streamer chamber [41], BNL experiments E802 [42], E895 [43,39], E877 [44].

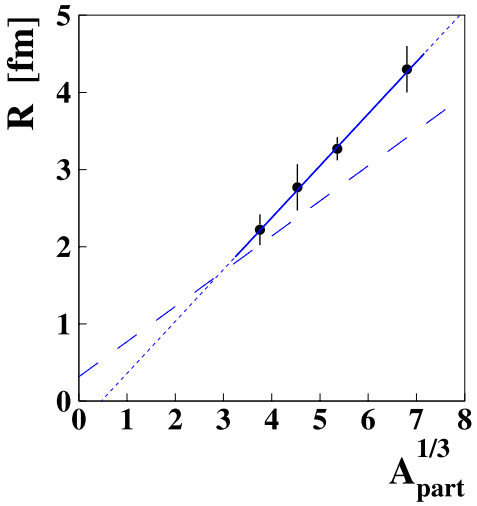


**Fig. 6.** The Gaussian source radius taken at $1.93A$ GeV from the excitation functions of the pp source radius (fig. 5, upper panel) *vs.* the cube root of the number of participating nucleons (full circles). The solid line is a linear regression to the data points. The dotted line is its extrapolation to small numbers of participants. The dashed line represents a similar dependence, but for $\Lambda$p correlation radii [6].

when interpreting the $\Lambda$p correlation radius which we derived recently for the same collision system, Ar+KCl at $1.76A$ GeV [6]. That dependence would give a minimum Gaussian radius of $(0.77 \pm 0.24)$ fm at $A_{part} = 1$. This trend is not only found for pp and $\Lambda$p correlations. Also for two-pion [1,33] and two-kaon [34] correlation radii derived from relativistic heavy-ion collisions such linear dependences with small intercepts have been reported.

## 5 Summary

Correlations at small relative momenta of pairs of protons, $\pi^+$ and $\pi^-$ mesons in central collisions of Ar+KCl at $1.76A$ GeV have been investigated with the large-acceptance spectrometer HADES. New results have been presented on the effective space-time extent of the proton and pion emission sources. Pions have been found to be emitted from apparently more extended sources than protons which, in turn, arise from slightly larger homogeneity regions than that derived from $\Lambda$p correlations. The beam energy and system size dependences of the emission sources have been studied. The present pp and $\pi\pi$ source radii do well complement existing data trends in the SIS energy range. The pp source radius at fixed beam energy has been found to increase with $A_{part}^{1/3}$. This finding points to a strong correlation of the emission source size with the overlap geometry. A lower limit of the pp correlation radius has been deduced from the extrapolation of this dependence down to the minimum number of participants. Both proton and pion source sizes clearly decrease with increasing impact parameter, further indicating a positive correlation of the correlation volume with the overlap volume of the colliding nuclei.

The HADES collaboration gratefully acknowledges the support by BMBF grants 06DR9059D, 06FY171, 06MT238 T5, and 06MT9156 TP5, by HGF VH-NG-330, by DFG EClust 153, by GSI TMKRUE, by the Hessian LOEWE initiative through HIC for FAIR (Germany), by grants MSMT LC07050 and GA ASCR IAA100480803 (Czech Rep.), by grant KBN 1P03B 056 26 (Poland), by grants FPA2006-09154 and CPAN:CSD2007-00042 (Spain), by grant UCY-10.3.11.12 (Cyprus), by CNRS/IN2P3 (France), by INFN (Italy), and by EU contracts RII3-CT-2005-515876 and HP2 227431.

## References


1. M.A. Lisa, S. Pratt, R. Soltz, U. Wiedemann, Annu. Rev. Nucl. Part. Sci. **55**, 357 (2005).
2. R.Q. Hanbury Brown, R. Twiss, Nature **178**, 1046 (1956).
3. G. Goldhaber, S. Goldhaber, W.-Y. Lee, A. Pais, Phys. Rev. **120**, 300 (1960).
4. S.E. Koonin, Phys. Lett. B **70**, 43 (1977).
5. M.G. Bowler, Z. Phys. C **39**, 81 (1988).
6. HADES Collaboration (G. Agakishiev *et al.*), Phys. Rev. C **82**, 021901 (2010).
7. HADES Collaboration (G. Agakichiev *et al.*), Phys. Rev. Lett. **98**, 052302 (2007).
8. A. Schmah, PhD thesis, Techn. Universität Darmstadt (2008).
9. HADES Collaboration (L. Fabbietti *et al.*), J. Phys. G: Nucl. Part. Phys. **36**, 064005 (2009).
10. HADES Collaboration (G. Agakishiev *et al.*), Eur. Phys. J. A **40**, 45 (2009).
11. HADES Collaboration (G. Agakishiev *et al.*), Phys. Rev. Lett. **103**, 132301 (2009).
12. HADES Collaboration (G. Agakishiev *et al.*), Phys. Rev. C **80**, 025209 (2009).
13. HADES Collaboration (G. Agakichiev *et al.*), Eur. Phys. J. A **41**, 243 (2009).
14. FOPI Collaboration (R. Kotte *et al.*), Z. Phys. A **359**, 47 (1997).
15. FOPI Collaboration (R. Kotte *et al.*), in *Proceedings of CRIS'98, Measuring the Size of Things in the Universe: HBT Interferometry and Heavy-ion Physics*, 2nd Catania Relativistic Ion Studies, Acicastello, Italy, June 8-12, 1998, World Scientific, p. 299.
16. FOPI Collaboration (R. Kotte *et al.*), Eur. Phys. J. A **6**, 185 (1999).
17. FOPI Collaboration (R. Kotte *et al.*), Eur. Phys. J. A **23**, 271 (2005).
18. FOPI Collaboration (B. Kämpfer *et al.*), Phys. Rev. C **48**, R955 (1993).
19. FOPI Collaboration (R. Kotte *et al.*), Phys. Rev. C **51**, 2686 (1995).
20. P. Danielewicz, G. Odyniec, Phys. Lett. B **157**, 146 (1985).
21. FOPI Collaboration (W. Reisdorf *et al.*), Phys. Rev. Lett. **92**, 232301 (2004).
22. HADES Collaboration (G. Agakishiev *et al.*), Eur. Phys. J. A **47**, 21 (2011).
23. GEANT 3.21, `http://consult.cern.ch/writeup/geant/` (1993).
24. I. Fröhlich *et al.*, Proceedings of Science, PoS(ACAT)076 (2007).
25. HADES Collaboration (P. Tlusty), *Proceedings of the XLVII International Winter Meeting on Nuclear Physics*, Bormio, Italy, Jan 26-30, 2009, Conf. Proc. SIF, Vol. **99** (SIF, Bologna, 2010) p. 243, arXiv:0906.2309.
26. Yu.M. Sinyukov, R. Lednicky, S.V. Akkelin, J. Pluta, B. Erazmus, Phys. Lett. B **432**, 248 (1998).
27. HADES Collaboration (G. Agakishiev *et al.*), Phys. Rev. C **82**, 044907 (2010).
28. S.A. Bass *et al.*, Prog. Part. Nucl. Phys. **41**, 255 (1998).
29. M. Bleicher *et al.*, J. Phys. G **25**, 1859 (1999).
30. J. Gosset, H.H. Gutbrod, W.G. Meyer, A.M. Poskanzer, A. Sandoval, R. Stock, G.D. Westfall, Phys. Rev. C **16**, 629 (1977).
31. S.Y. Panitkin, D.A. Brown, Phys. Rev. C **61**, 021901 (2000).
32. FOPI Collaboration (W. Reisdorf *et al.*), Nucl. Phys. A **848**, 366 (2010).
33. PHENIX Collaboration (S.S. Adler *et al.*), Phys. Rev. Lett. **93**, 152302 (2004).
34. PHENIX Collaboration (S. Afanasiev *et al.*), Phys. Rev. Lett. **103**, 142301 (2009).
35. N. Akhababian, J. Bartke, V.G. Grishin, M. Kowalski, Z. Phys. C **26**, 245 (1984).
36. M.A. Lisa *et al.*, Phys. Rev. Lett. **71**, 2863 (1993).
37. Plastic Ball (H.A. Gustafsson *et al.*), Phys. Rev. Lett. **53**, 544 (1984).
38. E895 Collaboration (S.Y. Panitkin *et al.*), *15th Winter Workshop on Nuclear Dynamics*, Park City, UT, Jan 9-16, 1999, arXiv:nucl-ex/9905008 (1999).
39. E895 Collaboration (P. Chung *et al.*), Phys. Rev. Lett. **91**, 162301 (2003).
40. W.A. Zajc *et al.*, Phys. Rev. C **29**, 2173 (1984).
41. LBL streamer chamber (D. Beavis, S.Y. Chu, S.Y. Fung, W. Gorn, D. Keane, R.T. Poe, G. VanDalen, M. Vient), Phys. Rev. C **28**, 2561 (1983).
42. E802 Collaboration (L. Ahle *et al.*), Phys. Rev. C **66**, 054906 (2002).
43. E895 Collaboration (S.Y. Panitkin *et al.*), Phys. Rev. Lett. **87**, 112304 (2001).
44. E877 Collaboration (D. Miskowiec *et al.*), Nucl. Phys. A **590**, 473c (1995).